JACS
JOURNAL OF THE AMERICAN CHEMICAL SOCIETY
Article
pubs.acs.org/JACS

Biomimetic Design of Mussel-Derived Bioactive Peptides for Dual-Functionalization of Titanium-Based Biomaterials

Guoqing Pan,*[,†] Shujin Sun,[†] Wen Zhang,[†] Ruobing Zhao,[‡] Wenguo Cui,[†] Fan He,[†] Lixin Huang,[†] Shih-Hui Lee,[‡] Kenneth J. Shea,[‡] Qin Shi,*[,†] and Huilin Yang*[,†]

[†]Department of Orthopaedics, The First Affiliated Hospital of Soochow University, Orthopaedic Institute, Soochow University, 188 Shizi Street, Suzhou, Jiangsu 215006, China

[‡]Department of Chemistry, University of California, Irvine, California 92697, United States

Supporting Information

ABSTRACT: Specific cell adhesion and osteogenicity are both crucial factors for the long-term success of titanium implants. In this work, two mussel-derived bioactive peptides were designed to one-step dual-biofunctionalization of titanium implants via robust catechol/TiO_2 coordinative interactions. The highly biomimetic peptides capped with integrin-targeted sequence or osteogenic growth sequence could efficiently improve the biocompatibilities of titanium implants and endow the implants with abilities to induce specific cell adhesion and enhanced osteogenicity. More importantly, rationally combined use of the two biomimetic peptides indicated an enhanced synergism on osteogenicity, osseointegration and finally the mechanical stability of Ti implants in vivo. Therefore, the highly biomimetic mussel-derived peptides and the dual-functional strategy in this study would provide a facile, safe, and effective means for improving clinical outcome of titanium-based medical implants.

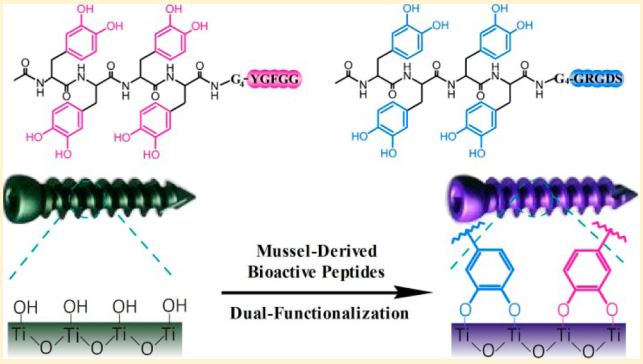

INTRODUCTION

Titanium (Ti) and its alloys are the most popular biomaterials for orthopedic and dental implants due to their excellent mechanical and chemical properties, high corrosion resistance and low allergenicity.[1] However, the general problem in Ti implants is the bioinertness and lack of bioactivities to induce specific cell and tissue responses (e.g., adhesion, signaling, and stimulation) for direct bone regeneration at the bone−implant interface.[2] Moreover, the bioinertness of bald titanium probably induces foreign-body reactions, which would deteriorate the initial bone-implant anchoring and eventually cause implant loosening and failure of the implant.[3] For bone implants, the formation of direct and stable bone-to-implant connection in the early stage (i.e., osseointegration) plays a very important role in the biological and clinical success of the implants.[1a,2] Therefore, ideal Ti implants in clinic should possess desirable bioactivity, in particular the ability to induce specific cell adhesion to enhance anchoring and stimulate osteogenic differentiation to accelerate interfacial bone regeneration, so as to promote early osseointegration in vivo and finally form a biologically stable connection between the implants and surrounding bone tissues.[4]

To date, various bioactive moieties (e.g., peptides, proteins, growth factors, and even ions) have been employed to modify Ti implants in order to induce specific cell response by means of physical adsorptions/entrapments or chemical conjugations.[1b,5] These approaches, however, are limited by their deficiencies.[6] Physical methods based on weak noncovalent bonds commonly result in serious molecular leakage and are unable to display long-term bioactivity. By comparison, chemical conjugations are much more stable. However, traditional chemical modifications mostly involve tedious chemical reactions as well as sophisticated technologies such as anodic oxidation, acid-etching, and ion-doping. Moreover, additional chemical bridge linkers probably induce chronic inflammatory response in vivo.[7] In this context, the exploration of simple, efficient and robust methods to decorate Ti surfaces with desirable bioactivity and with low or no toxicity remains an enormous challenge in biomaterial science and is of great significance in clinical medicine.

In nature, marine mussels use a variety of catecholic amino acid (3,4-dihydroxy-L-phenylalanine, DOPA) rich proteins (*Mytilus edulis* foot proteins, Mfps, Figure 1a) to adhere to virtually all kinds of substrates under wet conditions,[8] due to the easy formation of covalent bindings as well as noncovalent interactions between substrates and the catechol groups of DOPA.[9] One particular instance is the strong coordination interaction between catechol group and titanium oxide.[10] Fortunately, titanium and its alloys are quickly sealed on the surface with a tight and continuous titanium oxide layer (TiO_2, 2−10 nm) in air.[11] Thus, rational design of catechol-containing

Received: September 22, 2016
Published: October 25, 2016

DOI: 10.1021/jacs.6b09770
J. Am. Chem. Soc. 2016, 138, 15078−15086

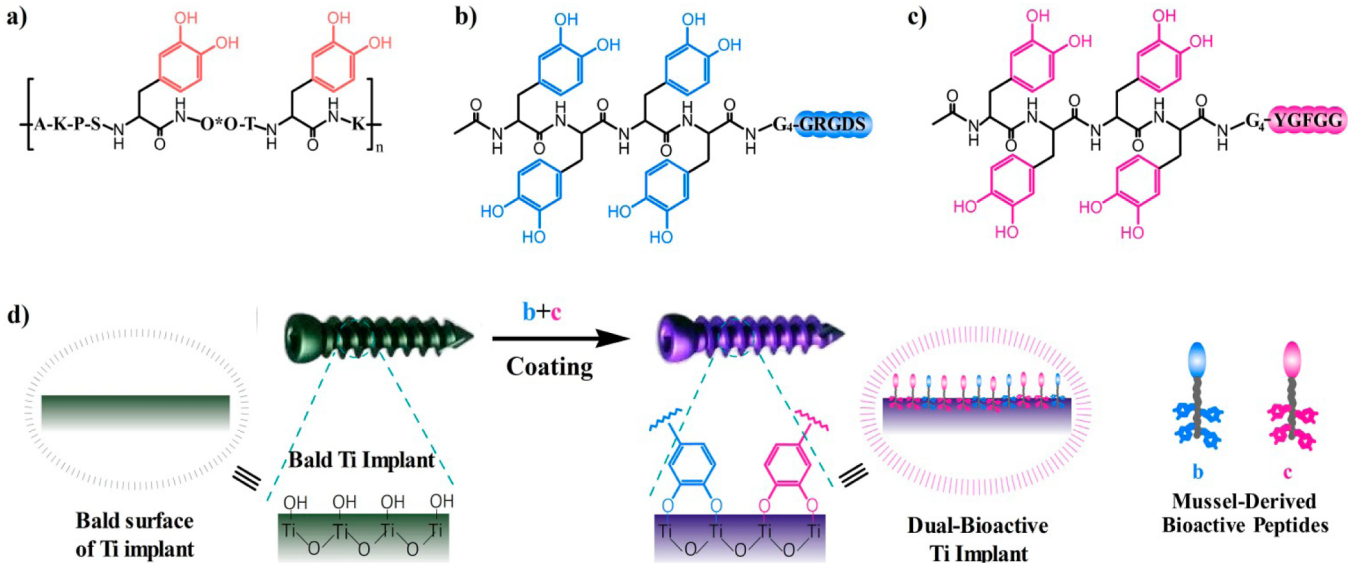

Figure 1. (a) Structural formula of the representative mussel foot proteins (Mfp-1) showing the catechol groups in their side chains. (b, c) Biomimicry of mussel-derived peptides with catechol groups in their side chains and bioactive motifs in the end ($(DOPA)_4$-G_4-GRGDS and $(DOPA)_4$-G_4-YGFGG). (d) Coordinative interactions between catechol group and titanium oxide for surface dual-biomodification of representative Ti implant (a cortical bone screw) by using the mussel-derived peptides (b) and (c).

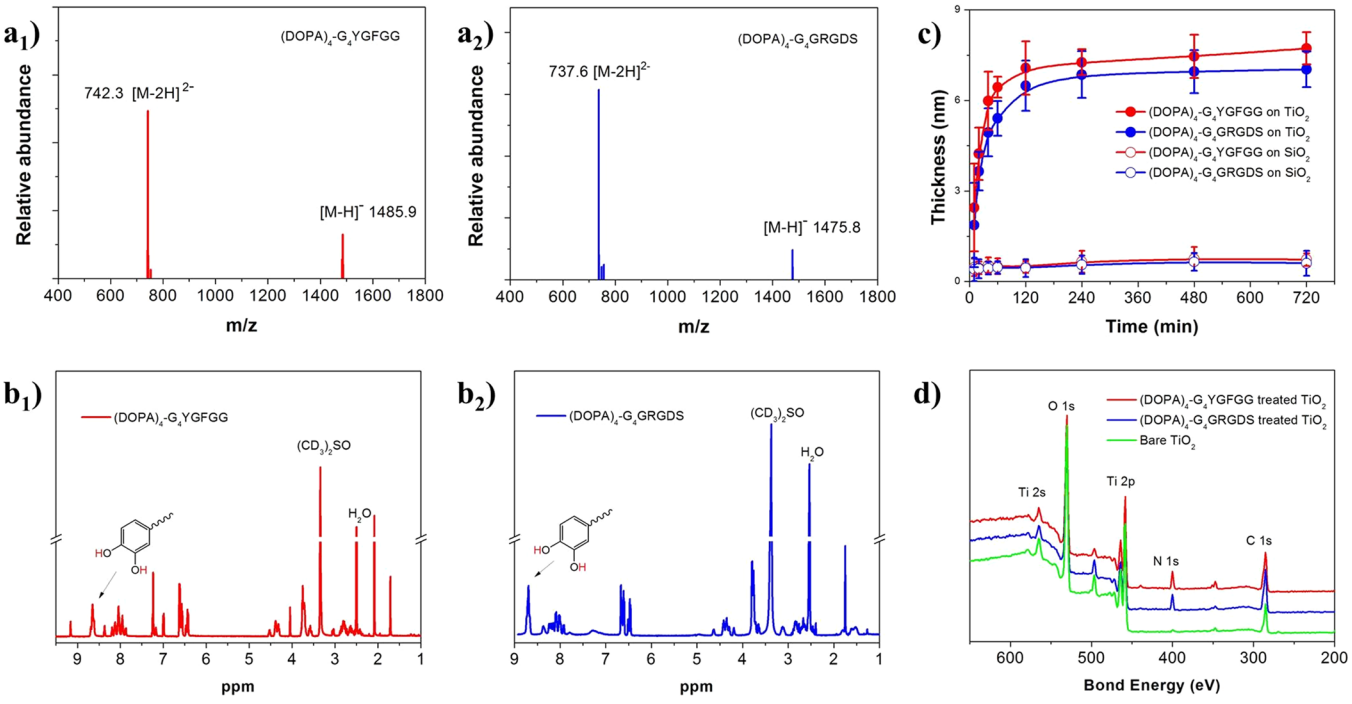

Figure 2. ESI mass spectrum (a) and ^{1}H NMR spectrum (b) of $(DOPA)_4$-G_4-YGFGG and $(DOPA)_4$-G_4-GRGDS. (c) Time-dependent thickness of the coordinatively bound peptides on a TiO_2-coated quartz substrate determined by ellipsometry. Peptide concentration was 0.01 mg·mL^{-1} in PBS, 25 °C. (d) X-ray photoelectron spectrum (XPS) of the bare TiO_2 surface and modified TiO_2 surfaces after 2 h of incubation in mussel-derived peptides (0.01 mg·mL^{-1} in PBS, 25 °C).

biomolecules for one-step modification of Ti implants is a more facile, flexible, and promising strategy compared to traditional chemical conjugations as well as the Mpfs protein fusion technology.[12] For example, DOPA-containing peptide/polymer complexes capped with cell adhesive[13] or osteogenic motifs[14] were recently designed for efficient coating Ti/TiO_2 surfaces. Such mussel-inspired bioactive molecules, however, are extremely rare and current studies were limited to in vitro cell response as well as monobioactivity. It is known that specific cell adhesion and osteogenicity on Ti implants are both crucial to bone regeneration at the bone-implant interface. Therefore, for this emerging strategy, rational modification of Ti implants with multibioactivity and high-biocompatibility to enhance in vivo osseointegration and biomechanical fixation is highly anticipated, and will be greatly helpful for clinical success of the established Ti implants.

Herein, we designed two mussel-derived peptides with different bioactivities for dual-functionalization of Ti implants

DOI: 10.1021/jacs.6b09770
J. Am. Chem. Soc. 2016, 138, 15078−15086

(Figure 1b and c). The mussel-derived peptides ((DOPA)$_4$-G$_4$-GRGDS and (DOPA)$_4$-G$_4$-YGFGG) both consist of a tetravalent catechol-containing (DOPA)$_4$ sequence, a quadri-glycine G$_4$ placeholder and a bioactive peptide sequence. In our design, the GRGDS peptide was mainly used for specific cell adhesion.[15] Also, the RGD sequence has been employed for surface modification of implants to promote early bone healing.[16] Another bioactive peptide YGFGG, derived from osteogenic growth peptide (OGP, an endogenous peptide present in mammalian serum[17]), was used for osteogenesis. As the active fragment of natural OGP, YGFGG has been frequently reported in its tethered state to regulate osteogenic differentiation.[14,18] Therefore, the two synthetic peptides with key bioactivities toward Ti implants were designed with highly biomimetic nature. Imaginably, a combined use of them could also endow Ti surfaces with desired dual-bioactivity, i.e., specific cell adhesion and osteogenicity. In this study, cell responses to the peptide-treated surfaces, in particular the impact of dual-biofunctionality on early osseointegration and biomechanical stability of Ti implants in vivo, were demonstrated for the first time. We anticipate that the highly biomimetic peptides for dual-bioactivation of Ti implants in this study would facilitate an improved clinical outcome of titanium-based medical implants.

RESULTS AND DISCUSSION

The mussel-derived bioactive peptides were prepared by standard Fmoc-based solid-phase peptide synthesis strategy (Scheme S1). To introduce DOPA units into the sequences, acetonide-protected Fmoc-DOPA(acetone)-OH was used.[19] Moreover, the final peptides were capped with an acetyl group at the N-terminal. After HPLC purification, the peptides were characterized with electrospray ionization mass spectrometry (ESI-MS). The monoisotopic mass $[M-H]^-$ of (DOPA)$_4$-G$_4$-YGFGG and (DOPA)$_4$-G$_4$-GRGDS were measured at 1485.89 and 1475.83, which were calculated to be 1485.47 and 1476.42, respectively (Figure 2a$_1$ and a$_2$). The chemical structures of the two biomimetic peptides were then confirmed by ^{1}H and ^{13}C NMR. The spectrum of ^{1}H NMR clearly indicated the present of DOPA units with a diagnostic peak at 8.65 ppm that belongs to catecholic hydrogens (Figure 2b$_1$ and b$_2$). Meanwhile, other characteristic peaks in the spectrum of ^{1}H and ^{13}C NMR matched perfectly with each amino acid sequence (see Figures S1−S4 and the details in the Supporting Information). These results demonstrated the successful synthesis of two biomimetic peptides with multiple DOPA units and different bioactive motifs.

Previous studies demonstrated that multivalent catechol-containing sequence could be easily and stably grafted onto TiO_2 surfaces through coordinative interactions.[14] We here employed TiO_2-coated quartz substrates for this test. As shown in Figure 2c, after 1 h of incubation in PBS containing the two mussel-derived bioactive peptides, the thickness of grafted peptide layer on TiO_2-coated substrates rapidly increased up to ∼6 nm (in PBS). Note that in dry state, the thickness of grafted peptide layer decreased to ∼4 nm. According to their molecular weights, the average peptide grafting densities of (DOPA)$_4$-G$_4$-YGFGG and (DOPA)$_4$-G$_4$-GRGDS were estimated to be 1.67 and 1.64 chains·nm^{-2} (see details in the Supporting Information), which was 1.6-fold as much as our previous method.[20] It is worth mentioning that the combined use of this two peptides in different ratios also showed similar surface densities ∼1.65 chains·nm^{-2} (i.e., 274 pmol·cm^{-2}). In contrast, the thickness of peptide layers on untreated surfaces (i.e., bare quartz) showed no significant increase under the same conditions, indicating the high-efficiency and selectively binding ability of the mussel-derived bioactive peptides toward TiO_2 surface. Surface elemental compositions were then characterized by XPS to further confirm the peptide immobilization. As shown in Figure 2d, significantly enhanced N 1s signal on peptide-treated TiO_2 surfaces was found at 400.12 eV, corresponding to the amide in peptide bonds. Quantitatively, the N/Ti atomic ratio increased from 0.058 (bare TiO_2) to around 0.50 (peptide treated TiO_2) after 2 h of incubation in peptide solutions (Table S1). These results, combined with the changes of static water contact angles after treatment (Figure S5), clearly confirmed the peptide immobilization on TiO_2 surfaces.

The availability of surface grafted peptides was then characterized by immunofluorescent assay (Table S2). Significant fluorescent signal could be observed on both of the two peptide-treated surfaces after incubation with their corresponding fluorescence-labeled antibodies. According to the surface fluorescent intensity, the amounts of bound antibodies on (DOPA)$_4$-G$_4$-YGFGG and (DOPA)$_4$-G$_4$-GRGDS-treated surface were estimated to be 38.6 and 40.8 pmol·cm^{-2}, respectively. This revealed that only ∼14% of the grafted peptides were available, probably due to the high peptide density (more than 1 chain·nm^{-2}) and yet relatively larger size of antibodies (several nanometers in three dimensions). It was also found that the peptide availability on surfaces treated with different peptide ratios showed no significant different, indicating the peptide densities on all the surfaces were high enough to achieve a saturated antibody binding. We then checked the durability of peptides after incubation of the peptide-treated TiO_2 substrates in Dulbecco's modified Eagle's medium (DMEM, pH = 7.4 at 25 °C) for 2 weeks. The intensity of N 1s signal in XPS only showed a reduction less than 20% (Figure S6 and Table S1). Furthermore, immunofluorescent assay was performed again to confirm the preservation of bioactivity. Despite of incubation in DMEM for 2 weeks, the amounts of bound antibodies on the peptide-treated TiO_2 surfaces did not show impressive reduction (Table S2). More convincingly, in the following cell adhesion experiments, we could observe excellent cell adhesion on this (DOPA)$_4$-G$_4$-GRGDS-treated surface in serum-free medium (see images in Figure S10 and detailed explanations below). These results suggested that the tetravalent coordinative interactions between catechol and TiO_2 in this study were stable enough to immobilize and preserve the bioactive motifs under approximately physiological condition, which is exactly the key factor for biomodified materials to efficiently display their bioactivities in vitro and in vivo.[3b]

As mentioned above, Ti implants that could induce specific cell adhesion and osteogenic signaling cascade are critical for early osseointegration in vivo.[1a,2] Thus, the TiO_2-coated substrates treated with different ratios of (DOPA)$_4$-G$_4$-YGFGG and (DOPA)$_4$-G$_4$-GRGDS were used to check the cell adhesive behavior and osteogenicity *in vitro*. Cell culture (human bone marrow-derived mesenchymal stem cells, BM-MSCs) on TiO_2-coated quartz substrate was first carried out to assess specific cell adhesion using medium with or without serum. Serum contains proteins that could be adsorbed on the surface and induce nonspecific cell adhesion,[21] thus serum-free condition is conducive to confirm the specific interactions

DOI: 10.1021/jacs.6b09770
J. Am. Chem. Soc. 2016, 138, 15078−15086

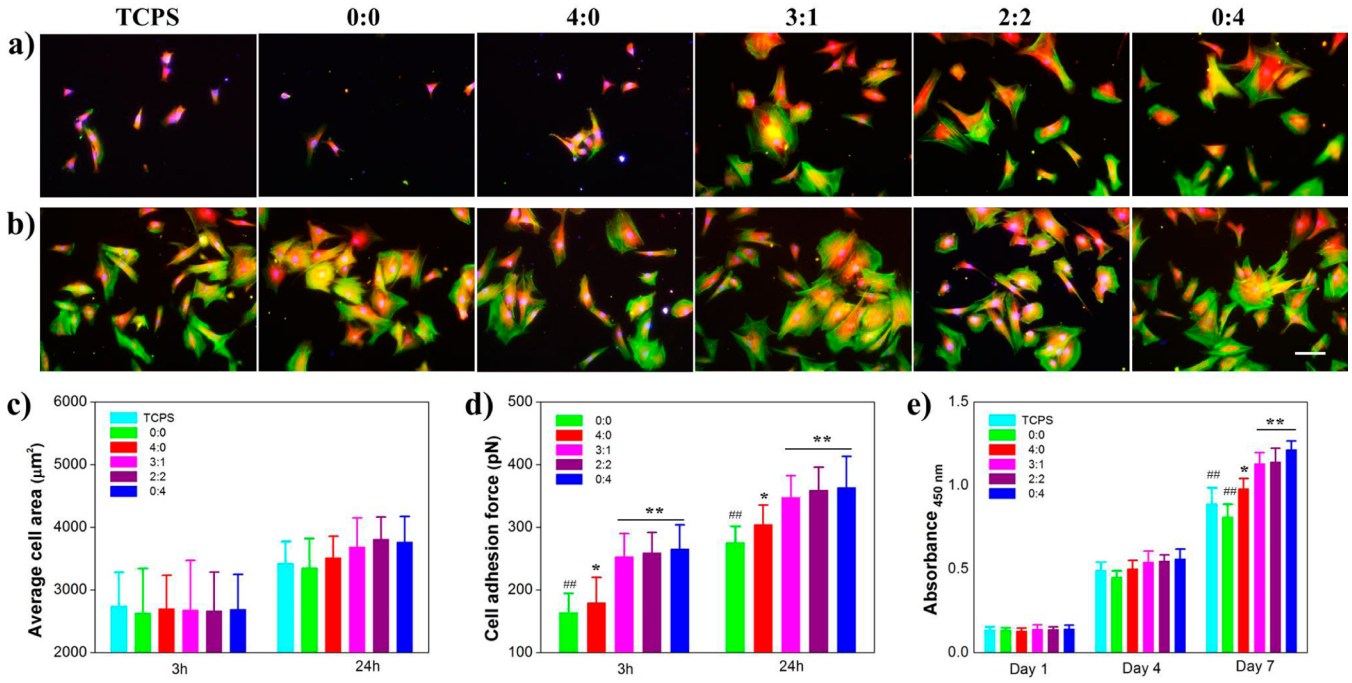

Figure 3. Biomimetic peptide-treated TiO_2 surfaces showed improved cell adhesion and proliferation behaviors. The morphologies of adherent cells after 3 h of culture in DMEM without (a) and with (b) fetal bovine serum (FBS, 10 vol %) on different surfaces (cell density, 4×10^4 cells per well). The cells were stained with DAPI (nuclei, blue), Alexa Fluor-488-conjugated phalloidin (actin filaments, green) and Alexa Fluor-555-conjugated antivinculin antibody (vinculin, red). Quantification of the average cell area (c) and cell adhesion force (d) after 3 and 24 h of culture on different surfaces. (e) Cell proliferation of BM-MSCs on different surfaces. For optimization of the surface biomodifications, the TiO_2-coated substrates were first incubated in PBS with different ratios of (DOPA)4-G4-YGFGG and (DOPA)4-G4-GRGDS (i.e., 0:0, 4:0, 3:1, 2:2, and 0:4, total concentration was 0.01 mg·mL^{-1}) for 6 h at room temperature. For each assay, TCPS and the bare TiO_2 surface (0:0) were both used as control. Data are presented as mean ± SD, $n = 4$. Statistically significant differences at the same period are indicated by $^*p < 0.05$ or $^{**}p < 0.01$ compared with bare TiO_2 surfaces, and $^{\#}p < 0.05$ or $^{\#\#}p < 0.01$ compared with the OGP/RGD (3:1) dual-treated surfaces. Scale bar = 100 μm.

between RGD motifs and integrin $\alpha_v\beta_3$, i.e., specific cell adhesion. The effects of TiO_2 surfaces on cell adhesion were investigated by F-actin cytoskeleton staining after 3 h of culture (Figures 3a and S7). The organization of F-actin networks for cells adhered to all the $(DOPA)_4$-G_4-GRGDS-treated TiO_2 surfaces (i.e., 3:1, 2:2, and 0:4) exhibited more spreading shape, regardless of the medium with or without serum. In addition, we could found clear vinculin plaques at the periphery of the cells (Figure S8), further demonstrating the excellent cell adhesion behavior in the RGD-containing groups. In contrast, adherent cells were rarely observed on bare TiO_2 (0:0), $(DOPA)_4$-G_4-YGFGG-treated TiO_2 (4:0), and TCPS plates when serum-free medium was used (Figure 3a), even after 24 h of cell culture (Figure S9). Furthermore, if the cells were blocked with a synthetic α_v integrin inhibitor Cilengitide before seeding,[22] adherent cells were also rarely observed on the $(DOPA)_4$-G_4-GRGDS-treated TiO_2 surfaces (Figure S10). Meanwhile, we also synthesized a control peptide with noncell-adhesive motif GRGES ($(DOPA)_4$-G_4-GRGES, see Figures S11–S13) for surface treatment. As expected, such nonbioactive peptide-treated surface showed poor cell adhesion behavior under serum-free condition (Figure S10). These findings together confirmed the specific integrin-regulated cell adhesion mechanism on the $(DOPA)_4$-G_4-GRGDS-treated surface.

Considering that practical use of an implant inevitably involved serum-containing condition, the cell adhesive behaviors in serum-containing medium were also investigated in detail. In serum-containing medium, all the surfaces exhibited efficient cell adhesion (Figure 3b). Moreover, their average cell spreading areas showed no significant difference even after 24 h of culture (~3500 μm^2, Figure 3c). Nevertheless, their relative cell adhesion forces, measured according to a previous centrifugation method,[23] were not the same. As shown in Figure 3d, the average cell adhesion forces on the RGD-containing TiO_2 surfaces reached to a relatively high value approximately to 355 pN, whereas the value decreased to 275 pN on a bare TiO_2 surface. The result indicated that the RGD-containing surfaces could efficient enhance cell anchorage, even under a serum-containing condition. This could be ascribed to the stable integrin-regulated cell adhesion mechanism, which is different from unstable and nonspecific cell adhesion caused by physical protein adsorption. It is worth mentioning that the $(DOPA)_4$-G_4-YGFGG-treated TiO_2 surface also showed a slight increase of adhesion force compared to the untreated one, probably due to the multivalent interactions between OGP peptides and OGP receptors on cell membrane. Taken together, the above findings confirmed that the biomimetic peptide-treated TiO_2 surfaces could induce specific cell recognition and enhance surface cell anchorage, which would be helpful for an implant to be identified as "autologous tissue" by the host[3b,24] and for the formation of stable connection between the Ti implants and surrounding bone tissues in vivo.

The lactate dehydrogenase (LDH) assay was further employed to quantify the cytotoxicity of the biomimetic peptides via measurement of LDH released from damaged cells.[25] As shown in Figure S14, all the peptide-treated TiO_2 surfaces exhibited significantly low cytotoxicity compared to the bare TiO_2 surface, indicating their improved cyto-compatibility that was comparable with TCPS controls. In addition, the cell

DOI: 10.1021/jacs.6b09770
J. Am. Chem. Soc. 2016, 138, 15078–15086

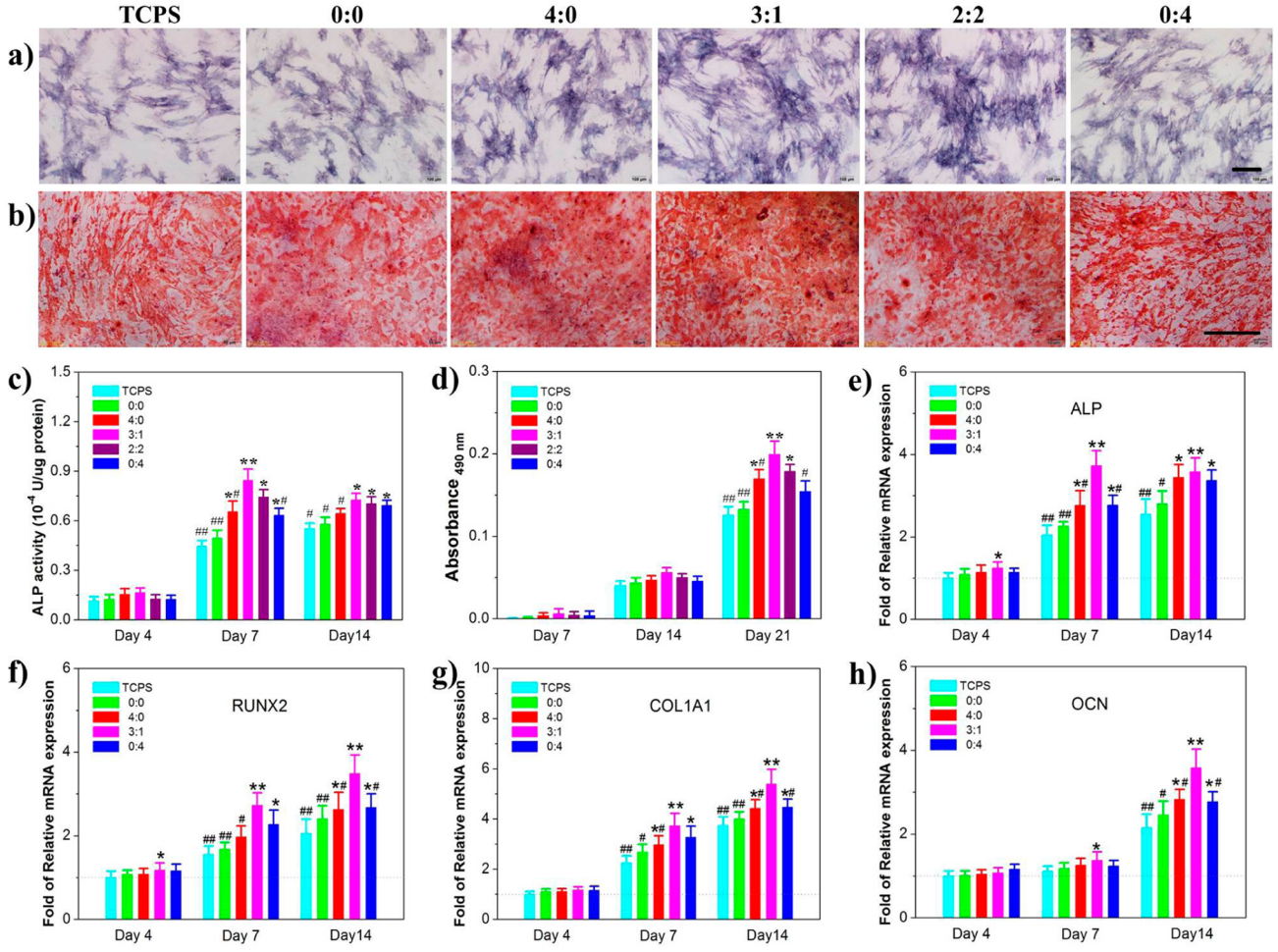

Figure 4. Biomimetic peptide-treated TiO_2 surfaces exhibited enhanced osteogenesis compared to the untreated surfaces in the osteogenic induction medium. (a) Representative images of ALP staining of BM-MSCs cultured on different surfaces after 7 days of culture in osteogenic induction medium. (b) Representative images of Alizarin Red S staining after 21 days of culture in osteogenic induction medium. (c) Quantitative ALP activity of BMSCs after 14 days of cultured in osteogenic induction medium. (d) Quantification of the Alizarin Red S stained mineral layer, dissolved in 1% hydrochloric acid, determined using a spectrophotometer. Osteoblast-related gene expressions of (e) ALP, (f) RUNX2, (g) COL1A1, and (h) OCN on different peptide-treated surfaces. The data were generated by real-time PCR and was presented as relative to control cells cultured in TCPS at fourth day by using normalization against a GAPDH reference. Data are presented as the mean ± SD, $n = 4$. Statistically significant differences at the same period are indicated by $^{*}p < 0.05$ or $^{**}p < 0.01$ compared with bare TiO_2 surfaces, and $^{\#}p < 0.05$ or $^{\#\#}p < 0.01$ compared with the OGP/RGD (3:1) dual-treated surfaces. Scale bar = 200 μm.

proliferation abilities on the above groups were measured by CCK-8 assay.[26] As shown in Figure 3e, all the peptide-treated groups show significant increase of proliferation after culture for 7 days as compared to the bare TiO_2. Moreover, the groups with RGD moieties (i.e., 3:1, 2:2, and 0:4) showed better cell growth than the group with YGFGG only (i.e., 4:0). These results demonstrated that (1) the biomimetic peptides could efficiently improve the cyto-compatibility of TiO_2 surfaces; (2) the TiO_2 surfaces with RGD moieties could greatly enhance specific cell adhesion and facilitate cell growth.

The effect of in vitro osteogenesis on the above peptide-treated TiO_2 surfaces was then investigated (Figure 4). Considering that the environment in vivo is inclined to induce osteogenesis in the area of bone defect,[27] osteogenic induction medium was used for in vitro osteogenic differentiation in this study. This would be a more reasonable reference for analyzing the effect of our mussel-derived bioactive peptides on in vitro and in vivo osteogenesis. The osteogenic differentiation of BM-MSCs was first characterized by the activity of alkaline phosphatase (ALP), an early marker for assessing osteoblastic metabolic activity.[28] After 7 days of culture in osteogenic induction medium, all the groups could elicit recognizable ALP-staining (Figure 4a). Quantitative analysis calculated by normalizing to protein contents showed that, all the peptide-treated groups displayed higher ALP activity throughout the observation period compared to bare TiO_2 groups and TCPS control (Figure 4c). More importantly, combination of the two biomimetic peptides could produce higher ALP activities as compared to the single one, probably due to the synergy of cell adhesive peptide RGD and osteogenic peptide YGFGG. For example, the two peptide-treated TiO_2 group (YGFGG/RGD, 3:1) exhibited a nearly 1.3-fold enhancement in ALP activity as compared to the groups treated with single peptide. Likewise, such enhanced osteogenesis was also observed in the later stages of differentiation. The matrix mineralization, caused by production of calcium binding proteins that can incorporate calcium ions into ECM in the later stages of mature osteoblast, was stained by Alizarin Red S after 21 days of culture (Figure 4b and d).[29] Semiquantitative analysis also indicated that the combination of YGFGG and RGD, especially at the ratio of 3:1,

DOI: 10.1021/jacs.6b09770
J. Am. Chem. Soc. 2016, 138, 15078−15086

could greatly increase matrix mineralization as compared to the single use of RGD or YGFGG. This result further confirmed the synergistic effect of YGFGG and RGD on osteogenesis. Not coincidentally, similar synergetic effect appeared frequently in materials with dual- or multibioactivity.[30] In our dual-functional groups, we speculated that RGD peptides provided sites for cell attachment to the substrate which enhanced the interaction of OGP-derived peptide with transmembrane receptors, thus leading to increased osteogenesis.

To further understand the state of BM-MSCs on different surfaces, the osteoblast-related gene expressions of alkaline phosphatase (ALP), runt-related transcription factor 2 (RUNX2), osteocalcin (OCN), and type I collagen (COL1A1) were analyzed by quantitative reverse transcription polymerase chain reaction (qRT-PCR). We first evaluated the osteoblast-related gene expressions under osteogenic induction condition (Figure 4e–h). For the dual-functional group, only the ratio of YGFGG and RGD at 3:1 was chosen due to the excellent promotion on ALP activity and matrix mineralization. Clearly, the mRNA expression of ALP on the dual-functional group was significantly higher than those on the untreated and single peptide-treated groups at day 4 and 7. In line with the ALP activity profiles, a decrease of ALP mRNA expression appeared on the dual-functional surface at day 14, which gave indirect evidence to an accelerated ECM mineralization and cell differentiation at this period.[31] RUNX2 is also a transcription factor necessary for early osteoblast differentiation.[32] Cells on the dual-functional surface exhibited the highest mRNA level of RUNX2 throughout the observation period, further suggesting its enhanced osteogenic differentiation at early stage. As an important marker for osteogenic differentiation, the gene expression of OCN is closely related to the later-stage extracellular matrix mineralization.[31] As expected, after 14 days of culture, the dual-functional surface exhibited significantly higher mRNA level of OCN compared to other groups. In addition, the dual-functional surface also showed dramatic increase in mRNA level of COL1A1 (the most abundant bone matrix protein) throughout the observation period. The enhanced gene expressions of OCN and COL1A1 jointly clarified the enhanced matrix mineralization of the dual-functional surface (Figure 4b) at the gene level.

We also used basal culture medium to investigate the real effect of our peptide on osteogenic gene expressions (Figures 5 and S15). Without auxiliary osteogenic inducing factors in medium, the level of osteogenic genes was directly related to the surface bioactivities. In addition, to clearly confirm the biofunction of immobilized OGP peptides for osteogenic differentiation, we also added a control group by using the $(DOPA)_4$-G_4-YGFGG-treated surface blocked with OGP antibody. After 2 weeks of culture, all the OGP-containing surfaces exhibited significant increase of the osteoblast-related gene expressions as compared to the untreated surface. This is similar to a previously reported result,[33] in which the tethered OGP peptide could significantly increase the osteogenic gene expressions of stem cells in a basal culture medium. In contrast, when the OGP-containing surface was blocked with OGP antibody, there was no significant increase in osteogenic gene expressions, reconfirming the OGP-mediated osteogenic differentiation in our system. In line with the results of qRT-PCR in osteogenic induction medium (Figure 4e–h), the dual-functional surface (YGFGG/RGD, 3:1) also induced the highest osteogenic gene expressions in basal culture medium. For example, the mRNA level of the later-stage marker OCN

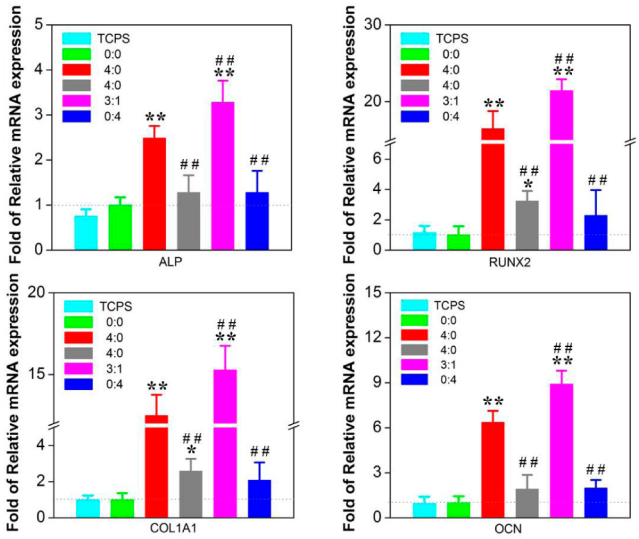

Figure 5. Osteoblast-related gene expressions on different peptide-treated surfaces after 2 weeks of culture in basal culture medium. The gray column referred to the $(DOPA)_4$-G_4-YGFGG-treated surfaces (4:0) blocked with OGP antibody. The data were generated by real-time PCR and was presented as relative to control cells cultured on untreated TO_2 surfaces (0:0) by using normalization against a GAPDH reference. Data are presented as the mean ± SD, $n = 4$. Statistically significant differences are indicated by $^{*}p < 0.05$ or $^{**}p < 0.01$ compared with bare TiO_2 surfaces (0:0), and $^{\#}p < 0.05$ or $^{\#\#}p < 0.01$ compared with the OGP-treated surfaces (4:0).

on the dual-functional surface was 1.4-, 4.5- and 8.9-fold higher than those of YGFGG-treated (4:0), RGD-treated (0:4) and untreated surfaces (0:0), respectively (Figure 5d). Note that, despite of the weak osteogenic ability of RGD-treated surface (0:4), the RGD motifs on the dual-functional surface also played an important role in osteogenic differentiation, probably due to the enhanced cell/material interaction and improved cell proliferation (Figure 3d and e). These findings, together with all the above in vitro results, definitely verified that the two mussel-derived bioactive peptides could efficiently decorate TiO_2 surfaces with desired bioactivities and improved cyto-compatibility. Moreover, due to the synergetic effect of integrin-targeted cell adhesion and OGP-mediated osteogenic differentiation, a facile dual-functional strategy could efficiently facilitate both adhesion and osteogenicity of BM-MSCs, suggesting its great potential to improve osseointegration of Ti implants in vivo.

We then performed *in vivo* experiments to check the practical efficacy of the biomimetic peptides for early osseointegration of Ti implants. Implantation of different titanium screws, including the peptide-treated groups and untreated controls, in the femoral condyles of New Zealand White rabbits was performed to demonstrate the proof-of-principle of this study (Figure S16a and b). To reduce the damage of surface peptide coatings as much as possible, a drill with diameter (1.5 mm) between the concave thread diameter (1.2 mm) and the convex thread diameter (2.0 mm) of the screw was chosen in the animal model (Figure S16c). Energy dispersive spectrometer (EDS) analysis revealed that the peptide-treated screws could efficiently preserve the coatings after the implantation (Figure S17). This is a prerequisite to investigate *in vivo* performance of the biomimetic peptides. After 4 weeks healing, the rabbit femoral condyles containing the implanted Ti screws were harvested, and the osteogenesis and osseointegration were then

DOI: 10.1021/jacs.6b09770
J. Am. Chem. Soc. 2016, 138, 15078–15086

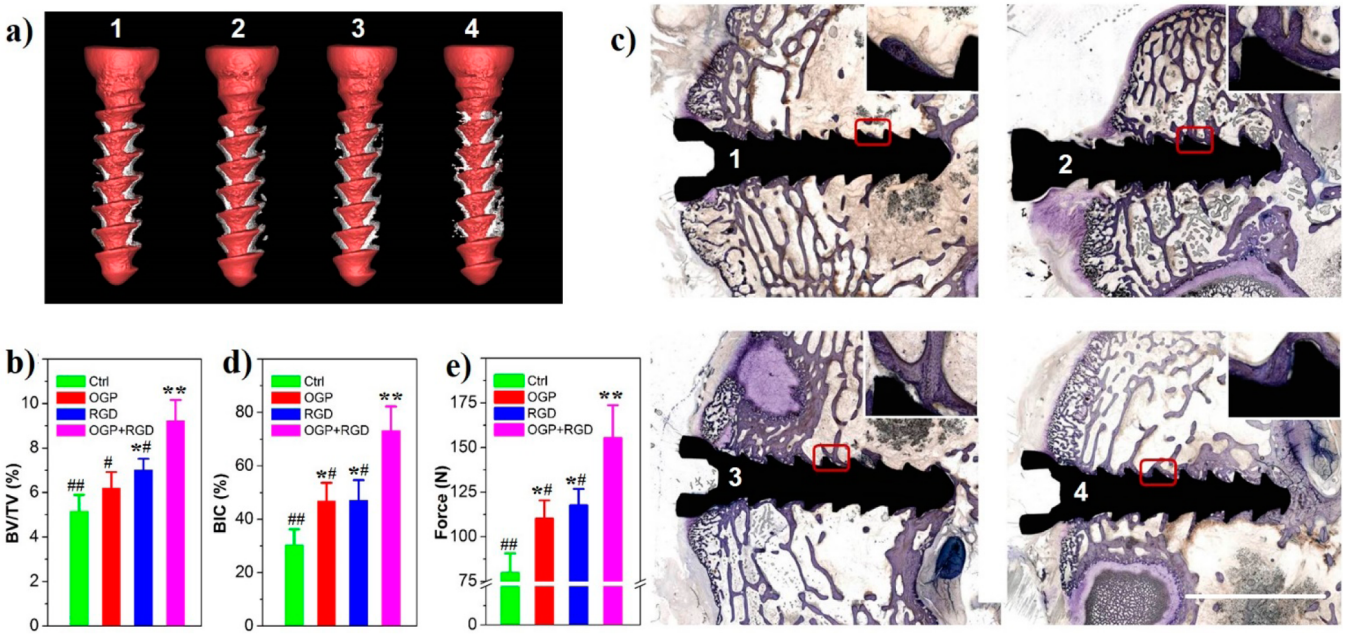

Figure 6. Peptide-treated screws exhibited enhanced osteogenesis and mechanical stability in vivo compared to untreated screws. (a) Micro-CT 3D reconstructed images and (b) quantitatively evaluating the peri-implant bone generation according to the percentage bone volume (BV) among tissue volume (TV) (BV/TV). (c) Representative histological images of titanium screws with toluidine blue stain. Insets in (c) show the magnified images in red boxes. (d) Average histomorphometric values of bone-implant contact (BIC). BIC was calculated as the percentage of implant's circumference that was in direct contact with bone mineral in histological sections. (e) Results of biomechanical pull-out testing. Implant nos. 1−4 refer to untreated (control), OGP-treated, RGD-treated, and OGP/RGD (3:1) dual-treated Ti screws, respectively. Data are presented as the mean ± SD, $n = 5$. Statistically significant differences are indicated by $^{*}p < 0.05$ or $^{**}p < 0.01$ compared with untreated controls and $^{\#}p < 0.05$ or $^{\#\#}p < 0.01$ compared with OGP/RGD dual-treated screws. Scale bar = 500 μm.

evaluated. 3D osteogenesis of each group was first evaluated by Micro-CT analysis (Figure 6a).[34] Under the same threshold and volume of interest (VOI) for CT scanning, the dual-functional Ti screws exhibited the highest percentage of bone volume to tissue volume (BV/TV, Figure 6b), which was in line with the result of osteogenic differentiation in vitro. Details in bone-implant interfaces were then investigated by histological staining.[35] Histological sections indicated that all the control and peptide-coated Ti screws showed no foreign-body giant cell formation or fibrous capsule at the bone-implant interfaces. More importantly, we can clearly observe contiguous bone matrix (blue stain) along the periphery of the dual-functional titanium screws (Figures 6c, S18, and S19). In contrast, less bone mineral was observed on the screws immobilized with single peptide RGD or YGFGG, and the least bone mineral was present on the untreated Ti screws. The bone-implant contact (BIC) determined by the percentage of the bone-implant apposition is the most intuitive property for evaluating osseointegration.[5i] Quantitative analysis of the histological sections revealed a nearly 1.5-fold enhancement in BIC on the dual-functional Ti screws (73.3 ± 8.9%) compared to the screws treated with single peptide (46.9 ± 6.7% and 47.2 ± 7.5% for screws immobilized with RGD and YGFGG, respectively) and more than 2-fold enhancement compared to the untreated screws (30.5 ± 5.7%), definitely demonstrating the excellent osseointegration of the dual-functional Ti screws (Figures 6d and S20). Moreover, the enhanced bone apposition on the peptide-coated Ti screws was further confirmed by EDS analysis of surface deposited calcium (Ca). The average atomic percentage of Ca was found to be higher on all the peptide-treated screws than that on untreated one after 4 weeks of implantation (Figure S21). Likewise, the dual-functional Ti screw exhibited the best bone apposition.

As known, stable connections between the implants and surrounding bone tissues are crucial to clinical success of Ti implants. Thus, the anchorage force of the Ti screws was evaluated by a biomechanical pull-out testing.[36] The results indicated significantly higher mechanical fixation of the peptide-coated screws compared to the untreated groups (Figures 6e and S22). More importantly, the dual-biofunctional Ti screws had the best stability, in which the average of maximum pull-out force (155.3 ± 18.5 N) exhibited nearly 2-fold enhancement as compared to that of the untreated ones (79.7 ± 10.9 N). It is worth mentioning that the RGD-coated screws also showed improved mechanical stability that was close to the OGP-coated one, probably due to the early integrin-regulated cell adhesion and subsequently improved osteoblastic proliferation on the surface in vivo. These in vivo results definitely demonstrated that the mussel-derived bioactive peptides could efficiently enhance the osteogenicity and osseointegration of Ti implants in vivo. In addition, combined use of the two peptides enable a greater quantity and continuity of peri-implant bone formation as well as improved mechanical fixation of the implants as compared to the use of single peptide, further suggesting the great promise of mussel-inspired biomimicry as a versatile and flexible strategy for Ti implant coating.

■ CONCLUSION

In summary, we have designed two novel mussel-derived bioactive peptides for facile biomodification of titanium implants through robust catechol/TiO_2 coordinative interactions. The high biomimetic peptides capped with integrin-targeted RGD sequence or OGP-derived osteogenic sequence

DOI: 10.1021/jacs.6b09770
J. Am. Chem. Soc. 2016, 138, 15078−15086

could efficiently improve the biocompatibility of titanium implants and endow the implants with desirable bioactivity, including both specific cell adhesion and osteogenicity. Moreover, rationally combined use of the two biomimetic peptides indicated an enhanced synergism on osteogenicity, osseointegration and finally the mechanical stability of Ti implants in vivo. Therefore, the highly biomimetic mussel-derived peptides and the dual-functional strategy in this study would provide a facile, safe and effective means for improving clinical outcome of titanium-based medical implants.

■ ASSOCIATED CONTENT

Supporting Information

The Supporting Information is available free of charge on the ACS Publications website at DOI: 10.1021/jacs.6b09770.

Materials and methods, supporting data; materials and synthesis procedures; NMR and ESI-MS data for different peptide sequences; characterization of TiO_2 surface and Ti screws; cell culture and animal experiments; H&E and micro-CT analysis; mechanical data and supplemental figures (PDF)

■ AUTHOR INFORMATION

Corresponding Authors

*yueer@suda.edu.cn (G.P.)
*shiqin@suda.edu.cn (Q.S.)
*hlyang@suda.edu.cn (H.Y.)

Notes

The authors declare no competing financial interest.

■ ACKNOWLEDGMENTS

We acknowledge the support from National Natural Science Foundation of China (Nos. 21574091, 51373112, 31400826, 31570978, and 81572131), Natural Science Foundation of Jiangsu Province (BK20160056 and BK20151210), Jiangsu Provincial Special Program of Medical Science (BL2012004), Jiangsu Provincial Clinical Orthopedic Center, and the Priority Academic Program Development of Jiangsu Higher Education Institutions (PAPD).

■ REFERENCES

(1) (a) Geetha, M.; Singh, A. K.; Asokamani, R.; Gogia, A. K. *Prog. Mater. Sci.* **2009**, *54*, 397−425. (b) Tejero, R.; Anitua, E.; Orive, G. *Prog. Polym. Sci.* **2014**, *39*, 1406−1447.

(2) (a) Le Guéhennec, L.; Soueidan, A.; Layrolle, P.; Amouriq, Y. *Dent. Mater.* **2007**, *23*, 844−854.

(3) (a) Gristina, A. G. *Clin. Orthop. Relat. Res.* **1994**, *298*, 106−118. (b) Anderson, J. M. *Annu. Rev. Mater. Res.* **2001**, *31*, 81−110. (c) Sakka, S.; Coulthard, P. *Med. Oral Patol. Oral Cir. Bucal* **2009**, *16*, e42−44. (d) Ulrich, S. D.; Seyler, T. M.; Bennett, D.; Delanois, R. E.; Saleh, K. J.; Thongtrangan, I.; Kuskowski, M.; Cheng, E. Y.; Sharkey, P. F.; Parvizi, J.; et al. *Int. Orthop.* **2008**, *32*, 597−604.

(4) Goodman, S. B.; Yao, Z.; Keeney, M.; Yang, F. *Biomaterials* **2013**, *34*, 3174−3183.

(5) (a) Sun, N.; Guo, Y.; Liu, W.; Densmore, M.; Shalhoub, V.; Erben, R. G.; Ye, L.; Lanske, B.; Yuan, Q. *Sci. Rep.* **2015**, *5*, 8304. (b) Alghamdi, H. S.; Bosco, R.; van den Beucken, J. J.; Walboomers, X. F.; Jansen, J. A. *Biomaterials* **2013**, *34*, 3747−3757. (c) Uchida, M.; Oyane, A.; Kim, H. M.; Kokubo, T.; Ito, A. *Adv. Mater.* **2004**, *16*, 1071−1074. (d) Shah, N. J.; Hyder, M. N.; Moskowitz, J. S.; Quadir, M. A.; Morton, S. W.; Seeherman, H. J.; Padera, R. F.; Spector, M.; Hammond, P. T. *Sci. Transl. Med.* **2013**, *5*, 191ra83−191ra83. (e) Ferris, D. M.; Moodie, G. D.; Dimond, P. M.; Giorani, C. W. D.; Ehrlich, M. G.; Valentini, R. F. *Biomaterials* **1999**, *20*, 2323−2331. (f) Petrie, T. A.; Raynor, J. E.; Reyes, C. D.; Burns, K. L.; Collard, D. M.; García, A. J. *Biomaterials* **2008**, *29*, 2849−2857. (g) Andersen, O. Z.; Offermanns, V.; Sillassen, M.; Almtoft, K. P.; Andersen, I. H.; Sørensen, S.; Jeppesen, C. S.; Kraft, D. C.; Bøttiger, J.; Rasse, M.; et al. *Biomaterials* **2013**, *34*, 5883−5890. (h) Guillot, R.; Gilde, F.; Becquart, P.; Sailhan, F.; Lapeyrere, A.; Logeart-Avramoglou, D.; Picart, C. *Biomaterials* **2013**, *34*, 5737−5746. (i) Alghamdi, H. S.; Bosco, R.; Both, S. K.; Iafisco, M.; Leeuwenburgh, S. C.; Jansen, J. A.; van den Beucken, J. J. *Biomaterials* **2014**, *35*, 5482−5490. (j) Li, Y.; Xiong, W.; Zhang, C.; Gao, B.; Guan, H.; Cheng, H.; Fu, J.; Li, F. *J. Biomed. Mater. Res., Part A* **2014**, *102*, 3939−3950.

(6) (a) Meyers, S. R.; Grinstaff, M. W. *Chem. Rev.* **2012**, *112*, 1615−1632. (b) Pan, G.; Guo, Q.; Ma, Y.; Yang, H.; Li, B. *Angew. Chem., Int. Ed.* **2013**, *52*, 6907−6911.

(7) Coleman, D.; King, R.; Andrade, J. *J. Biomed. Mater. Res.* **1974**, *8*, 199−211.

(8) (a) Lee, H.; Scherer, N. F.; Messersmith, P. B. *Proc. Natl. Acad. Sci. U. S. A.* **2006**, *103*, 12999−13003. (b) Wei, Q.; Becherer, T.; Noeske, P. L. M.; Grunwald, I.; Haag, R. *Adv. Mater.* **2014**, *26*, 2688−2693. (c) García-Fernández, L.; Cui, J.; Serrano, C.; Shafiq, Z.; Gropeanu, R. A.; Miguel, V. S.; Ramos, J. I.; Wang, M.; Auernhammer, G. K.; Ritz, S.; Golriz, A. A.; Berger, R.; Wagner, M.; del Campo, A. *Adv. Mater.* **2013**, *25*, 529−533.

(9) (a) Sedó, J.; Saiz-Poseu, J.; Busqué, F.; Ruiz-Molina, D. *Adv. Mater.* **2013**, *25*, 653−701. (b) Saiz-Poseu, J.; Sedó, J.; García, B.; Benaiges, C.; Parella, T.; Alibés, R.; Hernando, J.; Busqué, F.; Ruiz-Molina, D. *Adv. Mater.* **2013**, *25*, 2066−2070. (c) Ejima, H.; Richardson, J. J.; Liang, K.; Best, J. P.; van Koeverden, M. P.; Such, G. K.; Cui, J.; Caruso, F. *Science* **2013**, *341*, 154−157.

(10) Fichman, G.; Adler-Abramovich, L.; Manohar, S.; Mironi-Harpaz, I.; Guterman, T.; Seliktar, D.; Messersmith, P. B.; Gazit, E. *ACS Nano* **2014**, *8*, 7220−7228.

(11) Effah, E.; Bianco, P.; Ducheyne, P. *J. Biomed. Mater. Res.* **1995**, *29*, 73−80.

(12) (a) Hwang, D. S.; Sim, S. B.; Cha, H. J. *Biomaterials* **2007**, *28*, 4039−4046. (b) Kim, C. S.; Choi, Y. S.; Ko, W.; Seo, J. H.; Lee, J.; Cha, H. J. *Adv. Funct. Mater.* **2011**, *21*, 4101−4108.

(13) Pagel, M.; Hassert, R.; John, T.; Braun, K.; Wießler, M.; Abel, B.; Beck-Sickinger, A. G. *Angew. Chem., Int. Ed.* **2016**, *55*, 4826−4830.

(14) Tang, W.; Policastro, G. M.; Hua, G.; Guo, K.; Zhou, J.; Wesdemiotis, C.; Doll, G. L.; Becker, M. L. *J. Am. Chem. Soc.* **2014**, *136*, 16357−16367.

(15) (a) Ruoslahti, E.; Pierschbacher, M. D. *Science* **1987**, *238*, 491−497. (b) Pan, G.; Guo, B.; Ma, Y.; Cui, W.; He, F.; Li, B.; Yang, H.; Shea, K. J. *J. Am. Chem. Soc.* **2014**, *136*, 6203−6206.

(16) (a) Oya, K.; Tanaka, Y.; Saito, H.; Kurashima, K.; Nogi, K.; Tsutsumi, H.; Tsutsumi, Y.; Doi, H.; Nomura, N.; Hanawa, T. *Biomaterials* **2009**, *30*, 1281−1286. (b) Elmengaard, B.; Bechtold, J. E.; Søballe, K. *Biomaterials* **2005**, *26*, 3521−3526.

(17) Bab, I.; Gazit, D.; Chorev, M.; Muhlrad, A.; Shteyer, A.; Greenberg, Z.; Namdar, M.; Kahn, A. *EMBO J.* **1992**, *11*, 1867−1873.

(18) (a) Policastro, G. M.; Lin, F.; Smith Callahan, L. A.; Esterle, A.; Graham, M.; Sloan Stakleff, K.; Becker, M. L. *Biomacromolecules* **2015**, *16*, 1358−1371. (b) Panseri, S.; Russo, L.; Montesi, M.; Taraballi, F.; Cunha, C.; Marcacci, M.; Cipolla, L. *MedChemComm* **2014**, *5*, 899−903. (c) Policastro, G. M.; Becker, M. L. *Wiley Interdiscip. Rev. Nanomed. Nanobiotechnol.* **2016**, *8*, 449−464.

(19) Hu, B.-H.; Messersmith, P. B. *Tetrahedron Lett.* **2000**, *41*, 5795−5798.

(20) (a) Pan, G.; Zhang, Y.; Ma, Y.; Li, C.; Zhang, H. *Angew. Chem., Int. Ed.* **2011**, *50*, 11731−11734. (b) Pan, G.; Zhang, Y.; Guo, X.; Li, C.; Zhang, H. *Biosens. Bioelectron.* **2010**, *26*, 976−982.

(21) (a) Wei, Q.; Becherer, T.; Angioletti-Uberti, S.; Dzubiella, J.; Wischke, C.; Neffe, A. T.; Lendlein, A.; Ballauff, M.; Haag, R. *Angew. Chem., Int. Ed.* **2014**, *53*, 8004−8031. (b) Liao, J.; Zhu, Y.; Zhou, Z.; Chen, J.; Tan, G.; Ning, C.; Mao, C. *Angew. Chem.* **2014**, *126* (48), 13284−13288.

(22) Kim, J. W.; Cochran, F. V.; Cochran, J. R. *J. Am. Chem. Soc.* **2015**, *137*, 6−9.

DOI: 10.1021/jacs.6b09770
J. Am. Chem. Soc. 2016, 138, 15078−15086

(23) (a) Wu, J.; Mao, Z.; Gao, C. *Biomaterials* **2012**, *33*, 810−820. (b) Reyes, C. D.; García, A. J. *J. Biomed. Mater. Res., Part A* **2003**, *67*, 328−333.
(24) Keselowsky, B. G.; Bridges, A. W.; Burns, K. L.; Tate, C. C.; Babensee, J. E.; LaPlaca, M. C.; García, A. J. *Biomaterials* **2007**, *28*, 3626−3631.
(25) Wang, B.; Song, J.; Yuan, H.; Nie, C.; Lv, F.; Liu, L.; Wang, S. *Adv. Mater.* **2014**, *26*, 2371−2375.
(26) Cheng, L.; Sun, X.; Zhao, X.; Wang, L.; Yu, J.; Pan, G.; Li, B.; Yang, H.; Zhang, Y.; Cui, W. *Biomaterials* **2016**, *83*, 169−181.
(27) (a) Wegst, U. G.; Bai, H.; Saiz, E.; Tomsia, A. P.; Ritchie, R. O. *Nat. Mater.* **2015**, *14*, 23−36. (b) Robling, A. G.; Castillo, A. B.; Turner, C. H. *Annu. Rev. Biomed. Eng.* **2006**, *8*, 455−498.
(28) Keselowsky, B. G.; Collard, D. M.; García, A. J. *Proc. Natl. Acad. Sci. U. S. A.* **2005**, *102*, 5953−5957.
(29) Jeon, O.; Wolfson, D. W.; Alsberg, E. *Adv. Mater.* **2015**, *27*, 2216−2223.
(30) (a) Morgan, M. R.; Humphries, M. J.; Bass, M. D. *Nat. Rev. Mol. Cell Biol.* **2007**, *8*, 957−969. (b) Moore, N. M.; Lin, N. J.; Gallant, N. D.; Becker, M. L. *Acta Biomater.* **2011**, *7*, 2091−2100. (c) Ebara, M.; Yamato, M.; Aoyagi, T.; Kikuchi, A.; Sakai, K.; Okano, T. *Adv. Mater.* **2008**, *20*, 3034−3038. (d) Mehta, G.; Williams, C. M.; Alvarez, L.; Lesniewski, M.; Kamm, R. D.; Griffith, L. G. *Biomaterials* **2010**, *31*, 4657−4671.
(31) Tsigkou, O.; Jones, J. R.; Polak, J. M.; Stevens, M. M. *Biomaterials* **2009**, *30*, 3542−3550.
(32) Ducy, P.; Zhang, R.; Geoffroy, V.; Ridall, A. L.; Karsenty, G. *Cell* **1997**, *89*, 747−754.
(33) Polini, A.; Wang, J.; Bai, H.; Zhu, Y.; Tomsia, A. P.; Mao, C. *Biomater. Sci.* **2014**, *2*, 1779−1786.
(34) Jones, A. C.; Milthorpe, B.; Averdunk, H.; Limaye, A.; Senden, T. J.; Sakellariou, A.; Sheppard, A. P.; Sok, R. M.; Knackstedt, M. A.; Brandwood, A.; et al. *Biomaterials* **2004**, *25*, 4947−4954.
(35) Park, J.-W.; Kurashima, K.; Tustusmi, Y.; An, C.-H.; Suh, J.-Y.; Doi, H.; Nomura, N.; Noda, K.; Hanawa, T. *Acta Biomater.* **2011**, *7*, 3222−3229.
(36) Aparicio, C.; Padrós, A.; Gil, F.-J. *J. Mech. Behav. Biomed. Mater.* **2011**, *4*, 1672−1682.

DOI: 10.1021/jacs.6b09770
J. Am. Chem. Soc. 2016, 138, 15078−15086